In Memory of Professor Hsun HU

Textures of Materials

Proceedings of the Eleventh International Conference
on
Textures of Materials

Volume 2

ICOTOM-11

September 16-20, 1996
Xi'an, China

Edited by
Zhide LIANG
Liang ZUO
Youyi CHU

International Academic Publishers

TEXTURES IN INTERMETALLIC COMPOUNDS - EXPERIMENTS AND SIMULATIONS

D. Raabe, J. Fischer-Bühner, J. Ball, G. Gottstein

Institut für Metallkunde und Metallphysik,
RWTH Aachen, Kopernikusstr.14, 52056 Aachen, Germany

ABSTRACT

The texture and microstructure evolution during deformation and annealing of polycrystalline intermetallic compounds is reviewed. Three basic alloys are considered, namely, B2 ordered NiAl, B2 / DO_3 ordered Fe_3Al, and $L1_2$ ordered Ni_3AL. A broad variety of sample conditions was obtained conducting compression and rolling experiments at various homologous temperatures and static heat treatments of the deformed specimens. The textures were studied using the orientation distribution function. The microstructures were investigated using optical, scanning electron (SEM) and transmission electron microscopy (TEM). The microtextures were studied using electron back scattering diffraction (EBSD) experiments in the SEM (NiAl, Fe_3Al, Ni_3Al) and convergent beam electron diffraction (CBED) in the TEM (Ni_3Al). The deformation textures obtained in the low and intermediate temperature regime (no dynamic recrystallization) were simulated using Taylor models. Special emphasis was laid on studying the influence of the various families of active slip systems and their respective critical resolved shear stress (CRSS) on the texture. The textures observed in the high temperature regime after hot deformation (quenched) or static heat treatments are discussed in terms of recovery (RY), recrystallization (RX), and polygonization of rotated lattice regions adjacent to grain boundaries (rotational RX).

Keywords: Intermetallic compounds, rolling textures, annealing textures, Taylor simulation

INTRODUCTION

1. General Aspects

Intermetallic compounds have increasingly attracted attention owing to their potential use for both ambient (Fe_3Al) [1], and high temperature (HT) structural applications (NiAl [2], Ni_3Al [3]). One of the main problems encountered in this class of materials is their relatively low ductility at ambient temperature which entails insufficient low-temperature fracture toughness. Owing to the effects of stoichiometry and ternary additions considerable progress was made in ductilizing and strengthening the here addressed intermetallic alloys in their respective technical operation temperature regimes. Further substantial property optimization was attained through improved microstructure control. In Ni_3Al considerable insight into the underlying mechanisms of microstructure optimization was gained by relating texture to microstructure [4,5]. Hence, texture formation in this compound shall be discussed only briefly. However, much less corresponding work was carried out about the fundamentals of texture formation in Fe_3Al [6,7] and especially in NiAl [8-12].

Concerning polycrystal plasticity especially the type and number of slip systems that are active during large strain deformation is a point under debate [8-12]. Concerning annealing the influence of deformation microstructure and long range order on RX and RY phenomena is of relevance [13-15]. In this context the method of quantitative texture analysis combining both experiment and simulation provides a

convenient means of investigating microstructure evolution on a quantitative elementary scale [4-12,16,17]. Texture evolution during plastic deformation is directly connected with the displacement gradient tensor which results from the shear on the active slip systems. As was shown in a recent series of investigations this relation can be exploited for identifying active slip systems from characteristic deformation textures [6-10,16,17]. Studying annealing textures allows to distinguish primary RX from RY since the former process discontinuously changes the texture while the latter one preserves it. However, a more detailed analysis employing microtexture investigation is required for understanding phenomena such as in-situ recrystallization or the so called rotational RX [18].
Table 1 shows some main properties that are relevant for understanding the texture and microstructure of the here investigated intermetallics. The results are arranged according to their similarity with non-ordered materials. We shall thus in each chapter discuss first Ni_3Al (largest similarity), then Fe_3Al, and finally NiAl (weakest similarity).

Table 1 Main properties of polycrystalline intermetallic alloys that are relevant for texture interpretation.

alloys	Influence of plastic deformation on long range order	Dominant slip directions and planes for polycrystal deformation *	Domain formation during recrystallization
Ni_3Al ($L1_2$)	yes	<110>, {111} and {001}	no
Fe_3Al (B2 / DO_3)	yes	<111>, {110} and {112} <100>, {001} and {011}	yes
NiAl (B2)	no	<100>, {0kl}	no

* In this table only the slip systems that are most relevant for low and high temperature deformation of polycrystals are mentioned. Further details will be addressed in the ensuing chapters.

2. Ni_3Al

Most of the studies have addressed property improvements due to compositional deviations and microstructure optimization [e.g. 3]. Especially the enhancement of the ductility and of the temperature for the peak strength, T_{peak}, of Ni-based B doped $L1_2$ compounds was addressed. A series of papers has focused on the microstructure and texture evolution during large strain rolling deformation at ambient temperature and annealing of B doped Ni_3Al polycrystals [4,5]. Corresponding Taylor simulations were also published [8,17]. The current paper reviews the main results.

3. Fe_3Al

Due to the control of microstructure and composition, the properties of Fe_3Al based alloys were improved, especially the room temperature (RT) ductility and the strength at elevated temperatures [e.g. 1]. The investigation of the origin of rolling and annealing textures of Fe_3Al increasingly gains momentum. Concerning low temperature deformation it is under debate whether the activation of {110} or {112} slip planes prevails [6-8,16,19]. Concerning annealing the kinetics and the transition from RY to RX are not yet sufficiently understood [16,20]. This study concentrates on the investigation of the texture and microstructure evolution of polycrystalline Fe_3Al during rolling and annealing.

4. NiAl

Most studies concentrated on single crystals aiming at the improvement of RT ductility and HT strength [21]. In contrast to an enormous progress in RT ductilization of soft single crystals (A_g>25%) [22], the RT ductility of NiAl polycrystals is much lower (A_g = 0-3%). This is due to the violation of the von-Mises criterion, i.e. only three independent slip systems are provided by the <100>{0kl}-slip family [23]. Other slip systems seem to occur only under special situations (e.g. hydrostatic stress state [24], 'hard' single crystals [25]). With increasing temperature a transition to ductile behavior is observed, which is commonly attributed to the onset of diffusional processes [26]. The occurrence of extrusion textures and a

microstructure with a high fraction of low angle boundaries were discussed as reason for the relatively high ductility (A_G = 2-3%) of extruded polycrystals [27,28]. Thus it seems promising for improving the RT ductility of polycrystalline NiAl to combine composition control with microstructure and texture control.

Despite of the variety of texture investigations of the as extruded state only little is known about the mechanisms that govern microstructure and texture evolution in NiAl polycrystals. This is due to the respective intricate deformation history. A <111>-fibre deformation texture was predicted to develop during uniaxial compression by Relaxed-Constraints (RC) Taylor-simulations due to <100>-slip [8]. However, other authors reported the absence of texture evolution during uniaxial compression experiments on NiAl polycrystals at various temperatures. Based on a Full Constraints (FC) Taylor type rigid body rotation calculation it was contended that in case of (three independent) <100>-slip systems texture evolution cannot take place [12]. However, as shall be outlined in the ensuing chapters our own work clearly puts these stipulations into perspective [9-11]. It is the purpose of this paper to shed further light on the mechanisms controlling deformation texture, annealing texture and microstructure evolution in NiAl-polycrystals.

EXPERIMENTAL

Table 1 shows the analysis of the compounds. A detailed description of the sample preparation and experimental procedures is given elsewhere (Ni_3Al [4,5,17], Fe_3Al [6,7], NiAl [9-11]). In this paper only a few essential sample states were selected for the discussion out of a large variety of investigated alloys, deformations and annealing treatments. The present alloys were selected since their textures are believed to reflect the main features of the respective materials groups. For texture analysis, specimens were prepared from the homogeneously deformed mid-plane sections. Further details were described elsewhere for Ni_3Al [4,5,17], Fe_3Al [6,7], and NiAl [9-11]. The measured pole figures are listed in table 2.

Table 1 Chemical composition of the intermetallic alloys in at. %.

alloy	Al	Cr	Zr	Mo	Nb	C	B	balance
IC15 (Ni_3Al+B)	24	-	-	-	-	-	0.24	Ni
Fe_3Al	28	0.088	0.05	0.02	-	0.06	-	Fe
NiAl	49	«0.01	-	«0.01	-	«0.01	-	Ni

Table 2 Measured pole figures

alloy	IC15 (Ni_3Al+B)	Fe_3Al / Fe_3Al+Cr	NiAl
pole figures	{111} {200} {220} {311}	{220} {400} {224} {206}	{100} {110} {112}
radiation	$Cu_{K\alpha}$	$Mo_{K\alpha}$	$Co_{K\alpha}$

The orientation distribution functions (ODF) were derived by using a standard Fourier type inversion method [29]. Local textures were examined employing EBSD. Some experimental features are specific of the single material classes and require brief consideration:

NiAl : After the initial treatment the NiAl samples had a grain size of 140µm. Compression tests were carried out at 773K, 973K and 1173K at $\dot{\varepsilon} = 10^{-4}s^{-1}$. The samples were compressed up φ=120% (true strain) and quenched with helium. The starting material for the annealing studies was obtained from cast and hot-extruded material with comparable purity and an average grain size of 60µm. Annealing studies were carried out in air on specimens compressed at 773K (φ=120%). The samples were annealed in the range at 973K and 1173K for 120-5400s.

Fe_3Al : After the thermomechanical treatment the Fe_3Al alloys contained imperfect ordered B2 and DO_3 structured areas. The starting samples had a grain size of 200µm. They were warm rolled at 830-860K to

ε=80% ($\varepsilon=\Delta d/d_0$, d=sheet thickness). RX did not occur during warm rolling. Samples with 5at% Cr and C in solution were warm rolled annealed in a salt bath at 1023K and 1123K for 1-5000s.
Ni_3Al : The samples had a grain size of 25µm. The specimens were cold rolled (RT) to a maximum thickness reduction of ε=94%. Annealing was carried out within the range 3-30min. at 743K and 1023K.

RESULTS AND DISCUSSION

1. Ni_3Al

1.1 Microstructure and texture evolution during deformation

Fig. 1 shows the texture evolution during cold rolling. The deformation texture of Ni_3Al is a weak copper-type texture consisting mainly of the B ({011}<211>), C ({112}<111>) and S-component ({123}<486>). It is characterized by an anisotropic spread of B towards the Goss- and S. This feature can be explained in terms of the microstructure. Rolling of Ni_3Al is characterized by the formation of inhomogeneities [4,5]. Below ε=30% microbands appear. At intermediate strains a second set of microbands forms and with increasing strain the two sets link up to form a network. With increasing strain the dense arrangement of microbands confines slip to the progressively smaller space between the microbands and promotes the formation of copper- and brass-type shear bands. The latter shear bands prevail in the rolling microstructure. They consist of tiny equiaxed crystallites and carry extremely large strains and misorientations. Dislocation cell formation was not observed. Local texture analysis within brass-type shear bands yields orientations in the scatter of {112}<110>, {314}<485> and {638}<746>. The orientations in the matrix and in regions of dense microband clusters can be associated with {100}<011>, {111}<112>, {110}<100> and {112}<111>. The inhomogeneous microstructure at large strains affects the texture evolution such that a very large random texture component (60% background) and an extensive spread of the discrete texture components develop. The present texture reveals substantial similarities to that of brass and might thus indicate deformation twinning [30]. However, by using CBED Ball and Gottstein [4,5] clearly showed the absence of twins, but instead the presence various types of micro- and shear bands in the deformation microstructure.
An essential difference between the deformation structure of Ni_3Al and single phase alloys is the dislocation arrangement. Whereas even in metals with low stacking fault energy the dislocation mobility for non-planar slip is high enough to form a cellular structure, there is no indication of cell formation in Ni_3Al. Instead, forced planar slip leads to the formation of thin microbands, which demonstrates the strong slip localization in Ni_3Al. From detailed X-ray diffraction studies [4] we conclude that the passage of many dislocations on a slip plane greatly enhances the cross slip mobility of dislocations owing to a local reduction of long range order. Avalanches of local cross slip supposedly leads to the observed microbands [4]. The main features of the rolling textures are in good accord with simulations [17]. However, details like the anisotropic scatter of B are not covered by the model and hence not adequately predicted.

1.2 Microstructure and texture evolution during annealing

Fig. 2 shows the texture evolution during annealing [4]. The appearance of new orientations is already recognized after annealing for 3min. at 743K. While the C- and S-orientations of the deformation texture quickly vanish, the B-orientation simply shows an increased scatter with progressing annealing time. However, a completely recrystallized state is only established after annealing for 30min. at 1023K. The RX textures are very weak. An ODF analysis reveals that 90% of the volume are randomly oriented. Three texture components are invariably recognized after RX with the orientations close to {013}<100>, {102}<201>, and {112}<294>. Nucleation started preferentially at shear bands, microband intersections and microband/matrix interfaces. Single grain orientation measurements on partially RX material did neither support growth selection not oriented nucleation. The almost random RX texture of Ni_3Al is attributed to the high nucleation rate at deformation inhomogeneities in combination with a low grain boundary mobility. Model ODF calculations reveal that two RX components ({013}<100> and {012}<021>) are related to the B orientation by a 27°<332> rotation. The third RX component has a second order twin relationship, 38.9°<110>, to B. These results show that the brass texture component, which represents the main orientation within the shear bands, and annealing twin formation play an important role during RX of Ni_3Al.

2. Fe_3Al

2.1 Microstructure and texture evolution during deformation

The warm rolling textures of all investigated Fe_3Al alloys are in the center layer characterized by an increase of the α-fiber between {001}<110> and {111}<110> with a local minimum at {112}<110> (Fig. 3). After large reductions {111}<110> becomes the main component. In a series of recent papers [6,7,16,19] this texture evolution was explained in terms of combined activation of {110}<111> and {112}<111> slip. Comparing experimental warm rolling textures with corresponding RC Taylor simulations suggests that the CRSS of {110}<111> glide systems might exceed that of {112}<111> systems (Fig. 4). This is also advocated by comparing Fe_3Al to bcc rolling textures. Bcc metals reveal a similar CRSS of the involved slip systems. Their rolling textures typically reveal a stronger orientation density between {001}<110> and {112}<110> as compared to Fe_3Al.

2.2 Microstructure and texture evolution during annealing

Fig. 5 shows the β-fiber of a 80% warm rolled and annealed specimen after 200s and 1000s at 1123K. The texture is characterized by a strong decrease of {111}<110> and an increase of {111}<112> during annealing. After 200s at 1123K a state of partial reformation of the microstructure is observed. After 500s and 1000s the deformation microstructure is removed. In this case hence RX seems to prevail. RY does per definition not change the deformation texture. At a lower annealing temperature (1023K) the texture is preserved which advocates the prevalence of RY (Fig. 5). For clarifying the underlying mechanisms in this case the microtexture was studied in a state of partial reformation of the microstructure. A dominance of grain boundaries with a misorientation of 15°-22.5° was observed, which does not reflect typical RY. A possible explanation is the mechanism of rotation RX which was discussed for dynamically recrystallized Mg alloys [18]. The prevalence of RX at elevated and RY or rotation RX at lower homologous temperatures is in line with previous investigations [20].

3. NiAl

3.1 Microstructure and texture evolution during deformation

Deformation texture analysis has been carried out on specimens deformed in a temperature range where dynamic RX might be expected to occur and probably influence deformation textures. The microstructure after deformation at 773K is comprised of flat grains, while grain boundary serrations and the evolution of fine-grained areas are observed at elevated temperatures. An EBSD analysis of this microstructure [10,11] substantiated that the latter microstructure consists of a subgrain structure with only few recrystallized grains which hardly affect deformation texture evolution. Upon compression a <111>-fibre texture develops which sharpens with increasing strain and temperature Fig.6, Fig.7. Starting with a non <111>-texture (Fig.6a), this evolution is well pronounced even after a true strain of φ=36% (Fig. 6b,d). No remarkable influence of grain size and composition on this deformation texture evolution was observed [10,11]. As was stated in a recent comment [9] these results clearly disprove previous experimental data [12]. Deformation textures were simulated by means of a visco-plastic FC and RC Taylor model [31] (RC : ε_{21}, ε_{31} relaxed, 1 : compression-axis). While this relaxation is strictly valid only for the flat grain limit [32,33], which does not apply at low strains, the results provide at least information about the deformation texture evolution at large strains. The RC model (uniaxial compression, <100>-slip (Fig. 8a) predicts the evolution of a <111> texture. The accord of simulation and experiment substantiates that <100>-slip prevails during large strain deformation of polycrystalline material. However, <100>-slip provides only three independent modes of strain. Consequently, strain compatibility can be violated at grain boundaries. In this context it is essential to underline that EBSD data showed in some grains pronounced orientation gradients in the vicinity of the large angle grain boundaries (Fig. 9). This observation suggests the activation of additional slip systems close to grain boundaries for preserving strain compatibility.

In complementation of <100>{0kl}-slip, <110>-slip can also contribute at HT extrusion [34]. Moreover, the latter system dominates the deformation of 'hard' single crystals above ca. 570K and is responsible for the pronounced brittle-to-ductile transition (BDT) in this orientation [25]. Combining <110>{110}- and <100>{0kl}-slip provides five independent slip systems [35] as required for preserving compatibility

in polycrystal deformation. Hence it was discussed, that the BDT in polycrystals (ca. 300°C-400°C) is due to the additional activation of <110>-slip [2,23]. However, the role of <110>-slip is controversial. Instead it was proposed that a combination of slip and climb of <100>-dislocations provides the adaptation mechanisms at the grain boundaries [23, 26, 36, 37]. The FC model (uniaxial compression, <100>+<110>-slip, Fig. 8b) predicts as well the evolution of a <111> texture. The RC model was used with <100>+<110>-slip as well, leading to identical predictions as the RC model with <100>-slip. It is worth to emphasize that the increase in texture sharpness is much stronger in RC (both models) than in the FC model (Fig. 8c). Accordingly, a similar increase in texture sharpness with increasing temperature is observed in experiment (Fig. 7). It was observed that the predictions of the FC model were entirely insensitive to variations of the strain rate sensitivity and the CRSS ratio. These considerations lead us to the following suggestions: At low temperatures the activation of <110> slip is at the grain boundaries required for preserving compatibility. This is based on two assumptions. First, we observe gradients. Second, at low temperatures diffusion might not suffice to allow accommodation of large strain misfits. The observation of the experimental texture sharpening with increasing temperature can only be explained by a gradual transition from the FC to the RC deformation mode. This is interpreted in terms of a transition from <100>+<110>-slip at low temperature to <100>-slip and climb at elevated temperature. These conclusions are seemingly not in line with previous work and shall be discussed in detail later [10].

3.2 Microstructure and texture evolution during annealing

The here presented results cover two annealing states. First, the lowest annealing temperature where complete microstructure restoration was observed within reasonable time (90min, 973K; Fig. 10a). Second, a higher annealing temperature (3min , 1173K, Fig.10b). In both cases the microstructural change suggested RX. However, surprisingly no corresponding texture change was observed (Fig. 11). While RX per definition changes the texture it may be argued that RY instead of RX dominates the microstructural change observed. This interpretation advocates a mechanism similar to RX in situ. However, this interpretation is not in line with studies on RX kinetics of polycrystalline NiAl [38] which suggest nucleation and growth. Thus, EBSD was used to study the misorientations between neighboring grains. Microstructure restoration due to RY should result in a high fraction of low angle boundaries (LAB). Fig. 12 shows that the fraction of LAB is quite low in both cases. This does not seem to support RY. However, one must keep in mind that due to the observed pronounced orientation gradients in the deformed grains RY can possibly entail local misorientations in excess of 15°. Furthermore, EBSD reveals a remarkable difference between both annealed states: The fraction of misorientation angles <35° is considerably larger for the lower (≈55%) than for the higher annealing temperature (≈40%), (Fig. 7). These observations might suggest a transition in the mechanism dominating microstructure restoration with increasing temperature from RY to RX. This reminds of the study mentioned above [38] where a significant change in RX kinetics between 880K and 1000K was reported. The authors observed that this transition corresponded to a change in shape of the newly formed grains.

COMMON ASPECTS OF TEXTURES IN INTERMETALLIC COMPOUNDS

The large body of experimental and simulated data obtained in our Aachen lab, from which only a small fraction was shown in this paper, allows to review some aspects that characterize texture evolution in the various intermetallic alloys.

1. Deformation : Considerable progress was achieved by comparing experiment to simulated deformation textures. This method allows to identify slip systems that contribute to large strain polycrystal deformation and to draw conclusions about the influence of long range order on slip system selection and microstructure evolution.

2. Annealing : Progress in this field was achieved by employing local texture measurements for identifying whether RY or RX prevailed during annealing. The measurements suggest that special attention must be drawn to the influence of order (NiAl) and domain formation (Fe_3Al) on RX kinetics.

According to these various aspects of texture formation the following rough classification is suggested:

Ni_3Al based alloys have a relatively low ordering energy and identical slip systems as fcc materials (low temperature). Concerning the underlying physical mechanisms of texture formation they are thus in principle similar to conventional fcc materials such as brass (except for twinning). However, their textures are considerably weakened by the very inhomogeneous microstructure.
Fe_3Al based alloys have a relatively low ordering energy and similar active slip systems as bcc materials. However, especially their deformation textures are not similar to those of bcc materials which can be attributed to the CRSS relation among the slip families involved.
NiAl based alloys have a large ordering energy and a small number of slip systems. Consequently, these materials reveal the most significant differences when compared to textures of non ordered materials.

REFERENCES

1. C. G. McKamey, J. A. Horton & C. T. Liu, Journ. Mater. Res. 4 (1989), 1156.
2. D. B. Miracle, Acta metall. 39 (1991), 1457.
3. D.P. Pope & S.S. Ezz, Int. Met. Rev. 29, 136 (1984).
4. J. Ball & G. Gottstein, Intermetallics 1, 171 and 191 (1993); 2, 205 (1994); 3, 209 (1994)
5. G. Gottstein, P. Nagpal & W. Kim, Mater. Sci. and Eng. A108, 195 (1989).
6. D. Raabe & W. Mao, Philos. Mag. A 71 (1995), 805.
7. D. Raabe, Acta metall. 44 (1996), 937.
8. D. Raabe, Computational Materials Science, 3 (1994), 231
9. J. Fischer-Bühner, D. Raabe, P. Wagner & G. Gottstein : Scripta metall. 33 (1995) 1261.
10. J. Fischer-Bühner & G. Gottstein : soon to be published
11. G. Gottstein, E. Brünger, L. Löchte, J. Fischer-Bühner & D. Ponge, Proc. 16th. Riso Int. Symp., edited by N. Hansen et al, 1995, p. 37, Riso National Laboratory, Roskilde, Denmark
12. R.W. Margevicius & J.D. Cotton, Acta. metall., 43 (1995), 646.
13. D. G. Morris & M. A. Morris, Materials Science Forum 113-115 (1993), 599.
14. R.W. Cahn & H. Temp. Al. & Interm., ed. S.H. Wang, C.T. Liu, D.P. Pope, J.O. Stiegler, (1990) 245
15. F.J. Humphreys & M. Hatherly, Recrystall. and Related Annealing Phenom., Pergammon (1995).
16. D. Raabe & J. Keichel, Materials Science and Engin. A 203 (1995), 208.
17. D. Raabe, Acta metall. 43 (1995) 1531.
18. S. E. Ion, F. J. Humphreys & S. H. White, Acta metall., 30 (1982), 1909.
19. D. Raabe and J. Keichel & Z. Sun, Journal of Materials Science 31 (1996) 339-344.
20. D. G. Morris & M Leboeuf, Acta metall. 42 (1994), 1817.
21. D. B. Miracle & R. Darolia, Intermetallic Compounds : Vol.2, edited by J. H. Westbrook & R.L. Fleischer, 1994, p.53, John Wiley & Sons Ltd
22. V. I. Levit, I A. Bul, J. Hu & M. J. Kaufman, submitted to Scripta metall. mater., 1996
23. D. B. Miracle, Acta metall., 41 (1993), 649.
24. R. W. Margevicius & J. J. Lewandowski, Scripta metall., 29 (1993), 1651.
25. R. D. Field, D. F. Lahrmann & R. Darolia, Acta metall. mat., 39 (1991), 2951.
26. R. R. Bowman, R. D. Noebe, S. V. Raj & I. E. Locci, Met. Trans., 23A (1992), 1493.
27. K. Vedula, K. H. Hahn & B. Boulogne, Mat. Res. Soc. Symp. Proc., 133 (1989), 299.
28. M. Dollar, S. Dymek, S. J. Hwang & P. Nash, Met. Trans., 24A (1993), 1993.
29. M. Dahms & H. J. Bunge, J. Appl. Cryst. 22 (1989), 439.
30. S. G. Chowdhury, R. K. Ray and A. K. Jena : Scripta metall. 32 (1995) 213.
31. L. S. Tóth, P. Gilormini & J. J. Jonas, Acta metall., 36 (1988), 3077.
32. U. F. Kocks & H. Chandra: Acta metall. 30 (1982) 695.
33. U. F. Kocks : private communication. (1995).
34. J. D. Cotton, R. D. Noebe & M. J. Kaufman, Intermetallics, 1 (1993), 117
35. R Darolia, D. Lahrmann & R. D. Field, Scripta metall. mater. , 26 (1992), 1007
36. J. Cotton & R. D. Noebe, Met. Trans., 25A (1994), 2303
37. R. D. Noebe, R. R. Bowman & M. V. Nathal, Int. Mater. Rev., 38 (1993), 193.
38. G. R. Haff & E. M. Schulson, Met. Trans., 13A (1982), 1563.

FIGURES

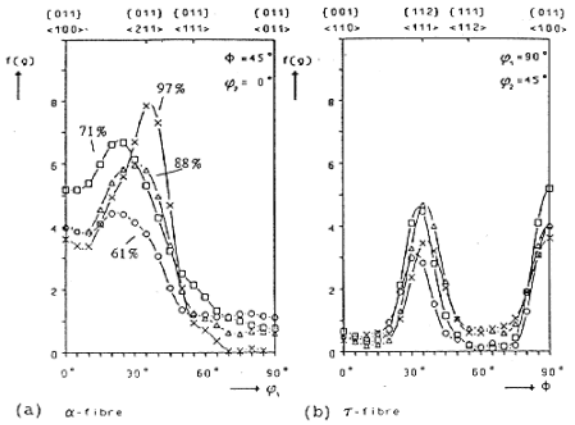

Fig. 1: Ni_3Al, cold rolling texture

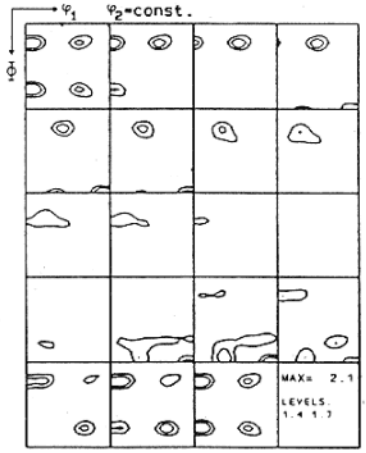

Fig. 2: Ni_3Al, annealing texture (85% cold rolled + 30 min. at 1013K)

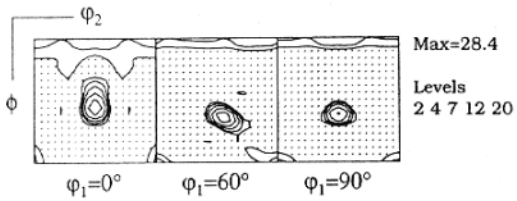

Fig. 3: Fe_3Al, cold rolling texture, ε=80%

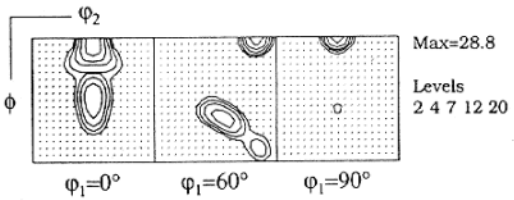

Fig. 4: Fe_3Al, Taylor simulation, details in [7]. (CRSS({110}<111>)= 10·CRSS({112}<111>)

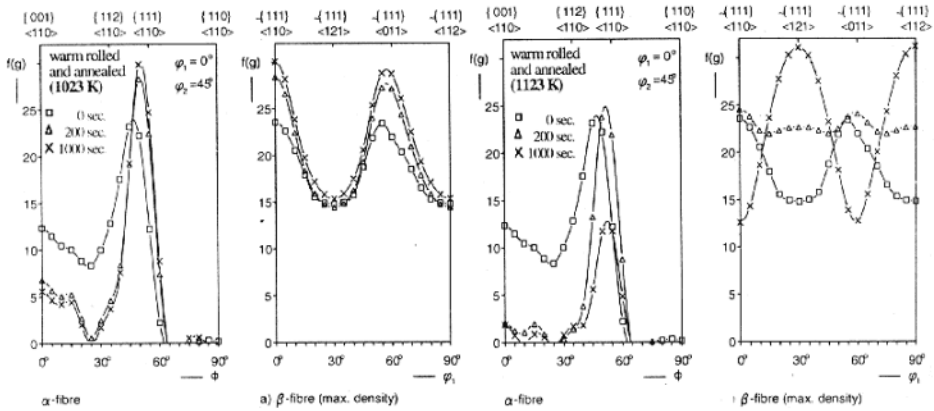

Fig. 5: Fe_3Al, annealing textures of the warm rolled Fe_3Al samples, center layer,

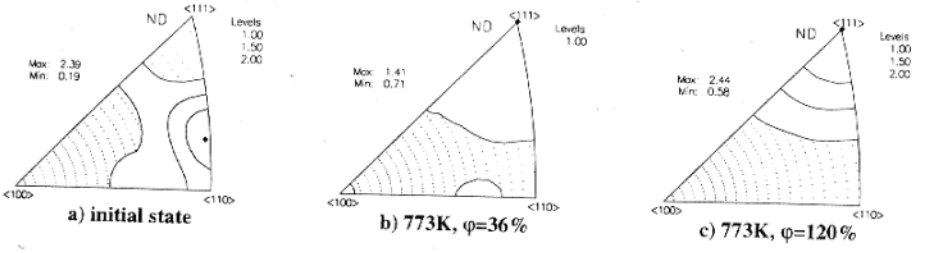

a) initial state b) 773K, φ=36 % c) 773K, φ=120 %

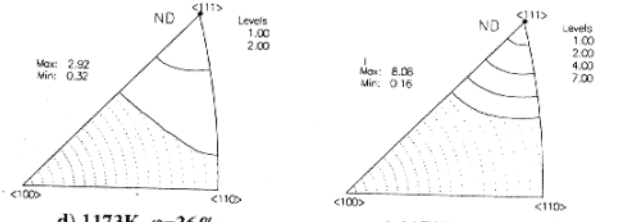

d) 1173K, φ=36 % e) 1173K, φ=120 %

Fig. 6: Experimental texture evolution during uniaxial compression deformation; inverse polefigures of the compression axis

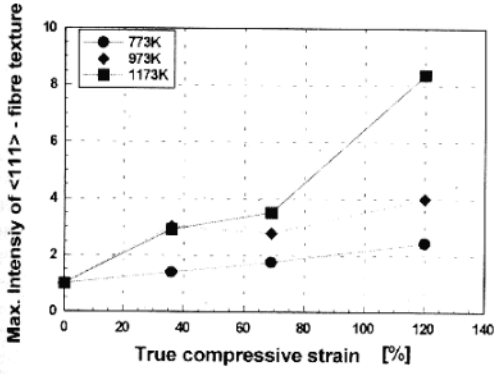

Fig. 7: Experimental texture evolution during uniaxial compression; max. intensity of the <111>-fibre component as a function of strain

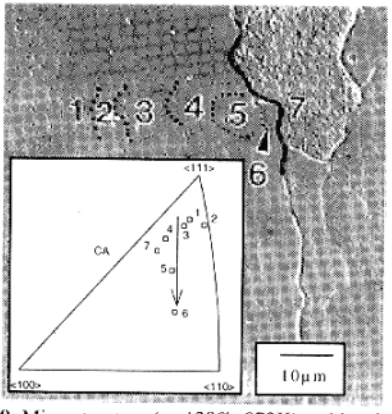

Fig. 9: Microstructure (φ=120%, 973K) and local orientations inside a former grain close to a grain boundary (dotted lines: low angle boundaries, dashed line: high angle boundary)

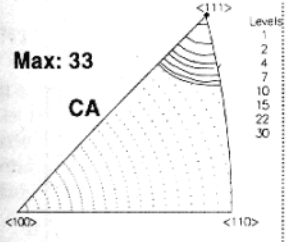

a) RC-model with assumption of {110}**<001>**- + {100}**<001>**-slip

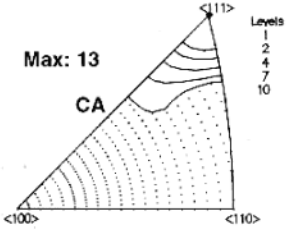

b) FC-model with assumption of {110}**<001>**-, {100}**<001>**- and {110}**<110>**-slip; $\tau_{<001>}/\tau_{<110>}=1/3$

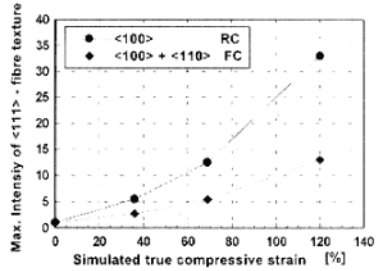

c) Max. intensity of the <111>-fibre as a function of simulated compressive strain

Fig. 8: Simulated compression texture evolution; a)+b): φ=120% ; inverse polefigures of the compression axis

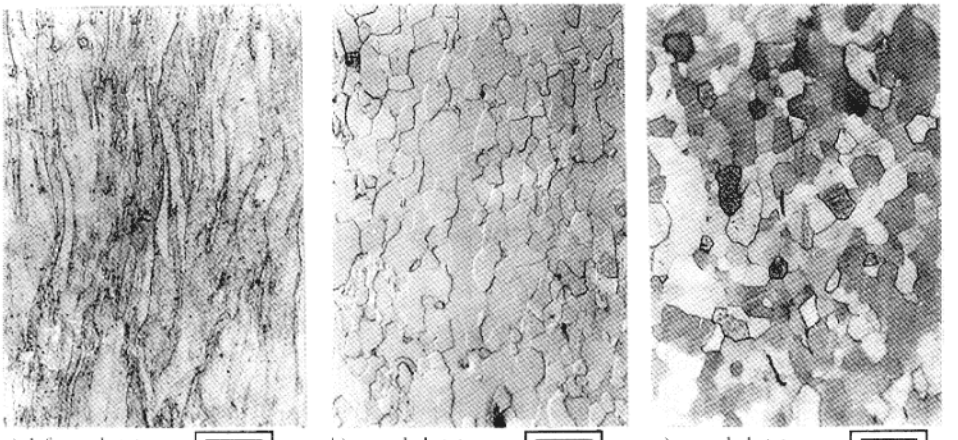

a) deformed state φ=120%, 773K

b) annealed state 90min 973K

c) annealed state 2min 1173K

Fig. 10: Microstructure after compression deformation and subsequent annealing treatment, compression axis ⇔

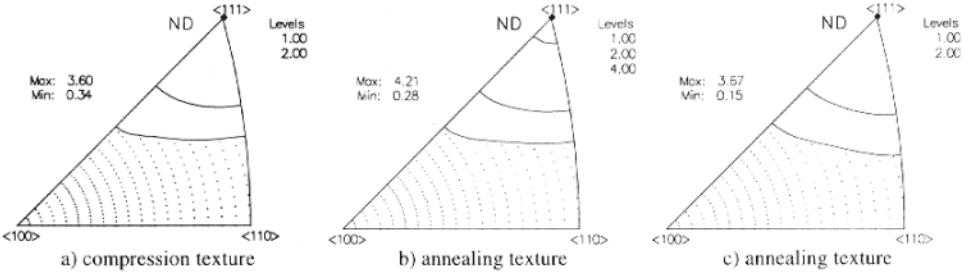

a) compression texture φ=120%, 773K

b) annealing texture 90min 973K

c) annealing texture 2min 1173K

Fig. 11: Experimental texture after compression deformation and subsequent annealing treatment; Inverse polefigures of the compression axis

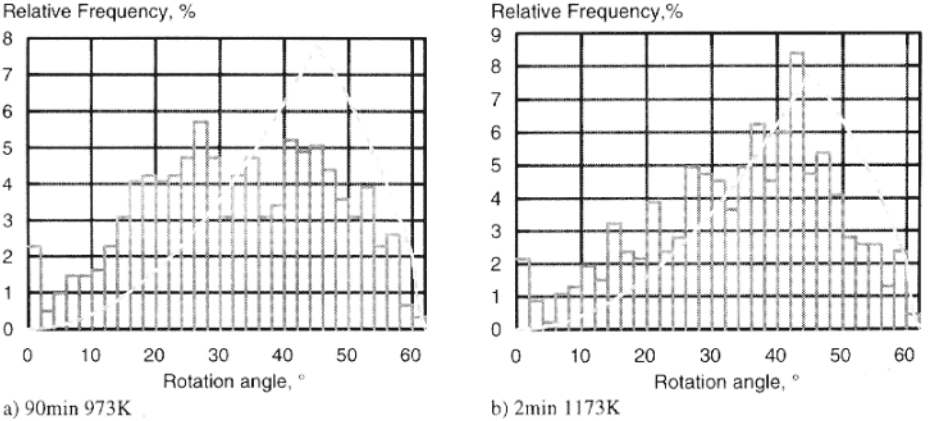

a) 90min 973K

b) 2min 1173K

Fig. 12: Distribution of misorientation angles between next neighbour grains in the annealed states (more than 200 grains / 500 misorientations analysed in each case)